Numerical modelling of vibropiling at the test site Altenwalde

Taisiya Pein [i)], Amir M. Kaynia[ii), iii)] Jan Hebig [i)]Volker Herwig [iv)]

i) Fraunhofer IWES, Am Fallturm 1, Bremen, Germany
ii) NTNU, Trondheim, Norway
iii) Norconsult, Sandvika, Norway
iv) RWE Renewables GmbH, Hamburg, Germany

ABSTRACT

This article describes characterization of a site for vibro-installation of large-diameter piles and estimation of soil parameters for the numerical code *VibPile* to simulate the vibratory pile installations. The code applies new computational models for the far field elastodynamic springs and accounts for the soil stiffness and damping outside and inside the pile. A minimum number of input soil parameters such as interface friction angle, shear wave velocity and soil density are required. Results of cone penetration test and shear wave velocity measurements in-situ were applied to estimate the input soil parameter and simulate the penetration of a large monopile with a diameter d=4.3m. The predicted optimum driving frequency is in good agreement with in-situ results.

Keywords: large diameter monopiles, vibratory driving, initial shear stiffness, damping

1 INTRODUCTION

Currently most wind turbines are supported by monopiles with diameters of up to 10 m. Vibratory piling installation techniques have several important advantages such as reduced noise level, speed of the installation process, and more reliable drivability for large diameter piles. However, most of the currently available drivability analysis and prediction tools are based on the approaches developed for solid low-diameter piles including axial stiffness (Novak, 1974) that are not fully applicable to the case of large-diameter hollow monopile cases.

This paper presents some results of the newly developed numerical code *VibPile* for simulation of the nonlinear dynamic response of large monopiles under harmonic loading and their installation by vibration (Kaynia et al. 2022). The novelty of the *VibPile* are the computational models for the far field elastodynamic springs and the accounting for the soil stiffness inside and outside of the pile and damping outside the pile.

The input parameters for the *VibPile* have a clear physical sense as they are the conventional interface friction angle φ to account for soil interface strength at pile tip and shaft as well as the shear wave velocity V_s and density ρ of the soil in the penetration depth for computation of the soil stiffness and damping. The interface friction angle is usually measured in the laboratory for specified relative densities. The shear wave velocity V_s can be estimated in-situ or derived from other measurements like cone penetration test CPT using published empirical relationships.

In this paper we describe the estimation of the input parameters needed for the code *VibPile* for a specified location in a thoroughly investigated test site Altenwalde. The focus is put on the estimation of shear wave velocity, for which published as well as site-specific empirical relationships were applied. The key features of the *VibPile* are summarized, the site conditions together with the pile parameters and a sensitivity study are described in the following chapters.

2 NUMERICAL CODE *VIBPILE*

The code uses pile geometry, hammer mass, excitation frequency, soil strength and stiffness along the pile shaft and at the pile tip as input parameters. *VibPile* is based on a nonlinear 1D FE model of the pile and pile-soil interaction along the wall and tip by

elasto-plastic springs representing the near field and elasto-dynamic elements (spring and dashpot) for the far field. For the side friction and tip resistance results from dedicated research or the classical engineering solutions, such as those by standards (e.g. API) and literature can be used. New computational models are developed for the far-field elastodynamic springs (Kaynia et al. 2022).

Unlike almost all existing solutions (see detailed review in Crispin and Mylonakis, 2021) *VibPile* is developed for hollow large-diameter pipe piles where the significant effect of waves in the soil inside the pile on the dynamic stiffness is considered. The pile shaft and pile tip stiffness and damping are functions of the soil's shear modulus and pile diameter. If no dedicated research is used for establishing the soil strength at the tip and on the pile shaft, one could use conventional parameters from the literature or standards as discussed below. In this case, the input soil parameters needed for the pile simulation are the shear wave velocity V_s, interface friction angle φ_{int}, and the soil density ρ.

2.1. Stiffness and damping

Dynamic stiffness and damping of the pile shaft and tip are calculated for the applicable frequency range as follows (Kaynia et al. 2022):

$$K_s = 4G = 4\rho {V_s}^2 \quad (1)$$

$$K_b = 6Gd = 6\rho {V_s}^2 d \quad (2)$$

$$D_s = 2Gd/V_s \quad (3)$$

$$D_b = 1.5Gd^2/V_s \quad (4)$$

Where d is the pile diameter, K and D denote stiffness and damping, the subscript s and b stands for the shaft and the base respectively.

2.2. Strength properties

Pile shaft resistance can be calculated following API:

$$f = \tan\varphi \cdot K_0 \cdot \sigma_0' \quad (5)$$

Where K_0- earth pressure at rest, ${\sigma_0}'$ - vertical effective stress, φ- interface friction angle between soil and pile.

The pile tip resistance is calculated from:

$$q_{tip} = {\sigma_0}' \cdot N_q \ (6)$$

Where N_q is a bearing capacity factor which depends on the interface friction angle:

$$\varphi' < 30° : \ N_q = 11.6\, tan^2(45° + \varphi/2) \tan\varphi \ (7)$$

The tip resistance is limited to:

$$q_{tip\,max} = 0.265\ MPa\ [tan\ (45° + \varphi\ /\ 2)]^{5.5} < 10\ MPa \ (8)$$

3 STUDY AREA AND PILE TESTING

Since 2014 the Altenwalde/Cuxhaven test pit located in northern Germany has been used for large scale geotechnical projects, such as monopile installation studies in Vibro-Project (Gattermann et al. 2015) with accompanying research and follow-up projects. Six monopiles with a diameter of 4.3 m and a length of 21 m were installed here. The area of the test pit was formed by Elsterian, Saalian and Weichsalian glacial periods. The geological history and recent sand excavation caused overconsolidation of the sandy deposits which are reflected in very high cone resistances up to 40 MPa. The sands present in the test field are saturated close below the surface.

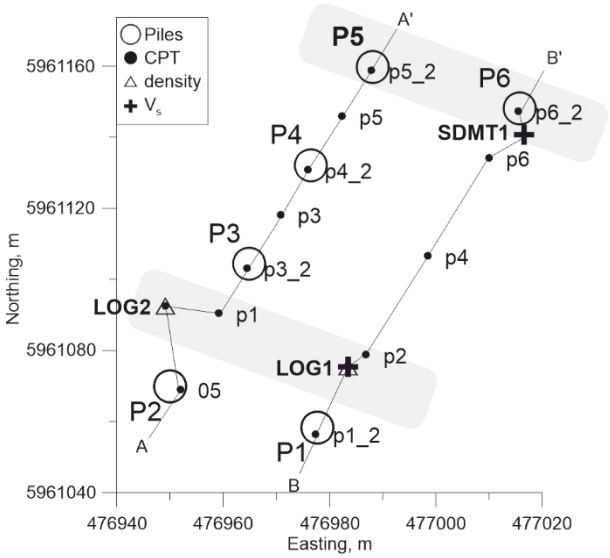

Figure 1. Overview over in-situ measurements and pile locations (PN). CPT data are available at all locations marked with a dot. Geophysical measurements are available at following locations LOG1: V_S measurement using P-S-log + SDMT, density; LOG2 – density; SMDT1 – V_S measurement. All these locations are used to derive a shear wave velocity profile at the pile P5 and are highlighted with grey rectangles. The CPT transects A-A' and B-B' used to correlate the local stratigraphy are shown on Figure 2.

Figure 1 provides an overview of the pile positions, the CPT investigations prior to pile installation and the velocity and density measurements. Shear wave velocities were measured at two locations LOG1 and P6. The SDMT was carried out at both locations until the depth of 20 m. At LOG1 a suspension P-S-logging test was carried out starting below the ground water level down to 38 m below ground level (mbgl). Gamma ray measurements are also available for sites LOG1 and LOG2. More details about velocity measurements can be found in Pein (2019)

In the following we use CPTu data, velocity and density measurements to specifically estimate the soil parameters at the location of the vibratory driven pile

P5 where high quality pile driving test data are available.

3.1 Pile parameters

The pile dimensions are given in Table 1.

Table 1. Dimensions of the pile P5

	Diameter, m	Wall thickness, m	Mass, t
P5	4.3	0.045	126

The pile was installed in two stages. In the current study we consider the second continuous driving stage starting at the depth of 9.5 m until the final installation depth of 18.80 m.

Table 2. Vibratory driving parameters for the pile P5

Penetration depth	m	< 9.5	>9.5
Frequency	Hz	12	22.5
Vibration power	bar	200-300	380
Continuous installation		no	yes
Net driving time	s	90	90
Reached embedded length	m	9.5	18.80

3.2 Laboratory measurements

The sand for laboratory testing recovered here is referred to as Cuxhaven Sand. It is a mixed sand from an outcrop of the Altenwalde sand pit. Laboratory tests (Biryaltseva et al. 2016) revealed homogeneous (in terms of minimum and maximum void ratios and grain size distribution) sand layers with granulometric curves comparable to typical North Sea sands. (Layers C, D, and F on Figure 2)

The peak friction angle and the interface friction angle was measured by Busch et al. (2022). For this, direct shear tests were undertaken under constant normal load on sand in contact with corroded as well as fresh steel pile pucks. The prepared sample void ratio $e \approx 0.54$ corresponds to Dr in the range $80 - 85\%$. The results presented in Table 3 were shown to be independent of the normal load.

Table 3. Interface and internal friction angle for Cuxhaven Sand

Friction angle	Internal Sand-to-sand	Sand-to fresh pile	Sand-to corroded pile
φ_{max}	45	23-33	40-45
φ_{cv}	35	20-30	25-30

3.3 CPTu and logging measurements

For this study 15 CPTu soundings, three V_s measurements and two density measurements were considered. Figure 2a) and b) shows the cone penetration tests taken along the transects A-A' and B-B'. Most of the CPTs reached the depth of 30 mbgl and reveal very high cone resistances (up to 40 MPa), an indication of overconsolidated aged sand. All CPT locations indicate numerous local heterogeneities at different scales caused by the glaciofluvial origin of the sediment. Six geological layers were identified using CPTu data in the study area. (Table 4). While the layers A, B, and C have a mainly constant thickness over the area, the thickness of the layer D increases towards North-East.

Table 4. Geological units

Unit	Description
A	Fine to medium Sand, dense, partially water saturated
B	Till, sand dominated, cohesive, partially water saturated
C	Fine to medium Sand, medium dense to dense, water saturated
D	Fine to medium Sand, dense to very dense, water saturated
E	Clayey sandy and pebbly till, water saturated
F	Fine Sand, dense to very dense, water saturated

For this reason, the velocity measurements from the locations LOG1 and P6 cannot be directly translated to the location P5. On Figure 2c the correlation of the CPT measurements, density logging and shear wave velocities are shown with the goal to identify intervals applicable for velocity- cone resistance correlation.

4 ESTIMATION OF V_S

The location closest to P5 with available shear wave velocity measurements is the location pile P6. As mentioned above due to dipping layer E and numerous local heterogeneities a direct translation of the shear wave velocity measured at the location LOG2 and P6 was considered to be insufficient. To estimate the V_s at the location p5_2 following equations were applied from Mayne (NCHRP and references therein) for sands:

$$Vs[m/s] = 277{q_t}^{0.13} \cdot {\sigma'_{v0}}^{0.27} \quad (11)$$

as well as for all soil types:

$$V_s = (10.1\, log q_t - 11.4)^{1.67}[f_s/q_t \cdot 100]^{0.3} \quad (12)$$

With q_t being the cone resistance, the f_s, the sleeve friction and the σ'_{v0} the vertical effective stress.

Additionally, a local simplified formula to estimate the shear wave velocity from q_c was derived. For this purpose, no distinction was made between different types of velocity measurements. The sequences of constant or monotonic V_s and q_c at both locations LOG1 and P6 were linearly correlated to each other resulting in the following relationship:

$$V_s[m/s] = 157.95 + 3.52 q_t[MPa] \quad (13)$$

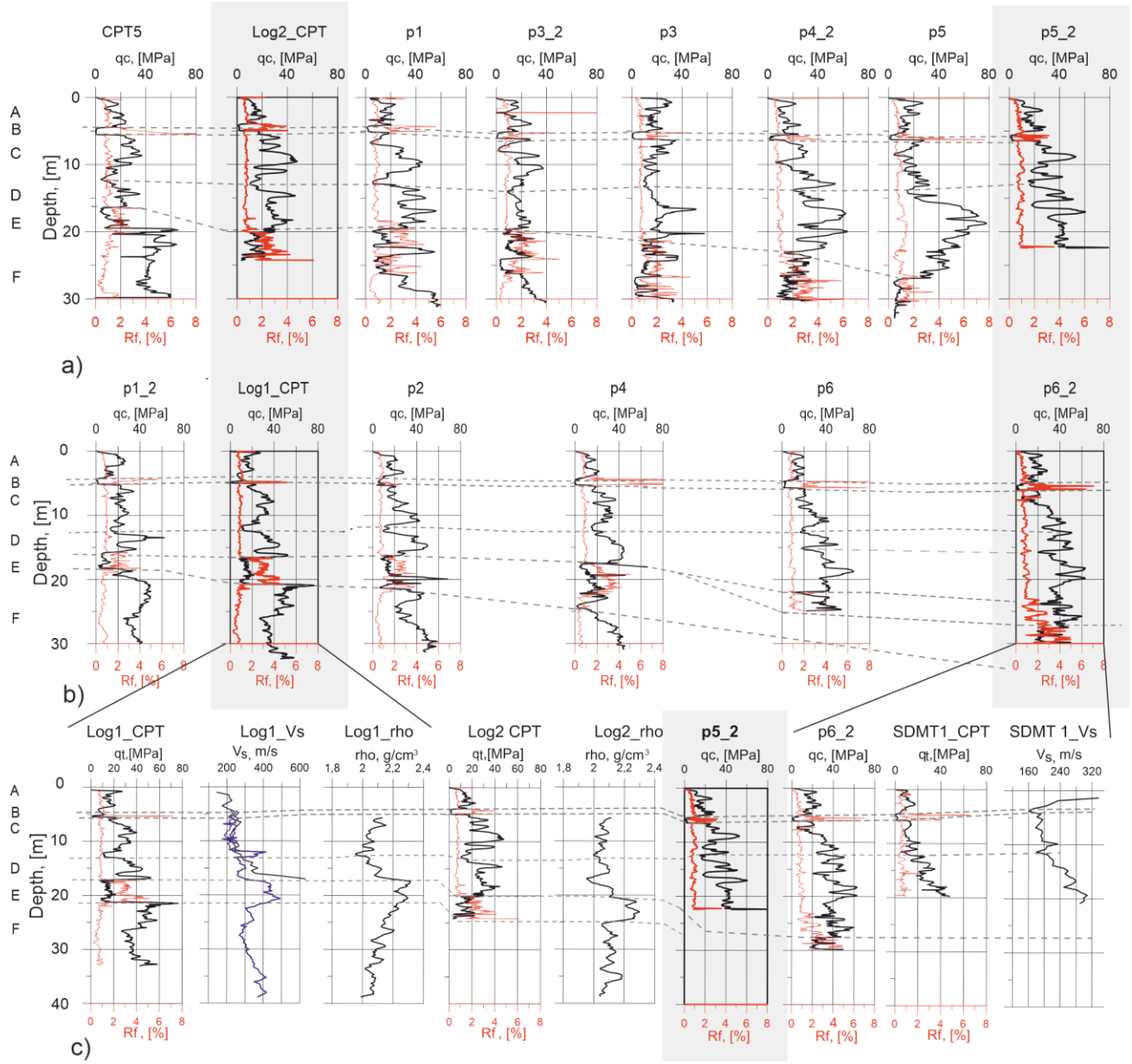

Figure 2. In-situ measurements in Altenwalde test pit. a) CPTu along Profile A-A'; b) CPTu along Profile B-B'(middle); c) correlation of the velocity, density and CPT measurements at the locations LOG1, LOG2, SDMT1 to the pile location of interest p5_2.

Figure 3 shows the comparison of estimated shear wave velocity by equations 11-13. The locally derived equation (13) predicts the measured data reasonably well; however, it should be noted that the very limited number of measurements may have led to overfitting.

Therefore, the general applicability of this expression has to be proven on other sites of comparable conditions. The equation (11) slightly overestimates the measurements and can be considered to provide the upper limit. The equation (12) overestimates the measurements up to 50% within the first 15 m but provides a good agreement with the measured data in clayey till and fine dense sands.

5 NUMERICAL SIMULATIONS

Using the obtained shear wave velocities, estimated density, the laboratory measured interface friction angle and assuming the coefficient of earth pressure at rest K_0=0.5 prediction of the driving rate was made using *VibPile* for the pile dimensions equal to the installed monopiles. Considering that the interface friction angle measured in the laboratory was independent of the normal load, the value was assumed constant over the whole profile length. (Table 5). As the excitation frequency in-situ is usually varied experimentally to achieve the optimal value, the frequencies close to the in-situ values were chosen. (Table 1)

Table 5. Input parameters kept constant over the pile length

Interface friction angle φ	25°
Earth pressure coefficient K_o	0.5
Density, ρ	2.0 g/cm^3

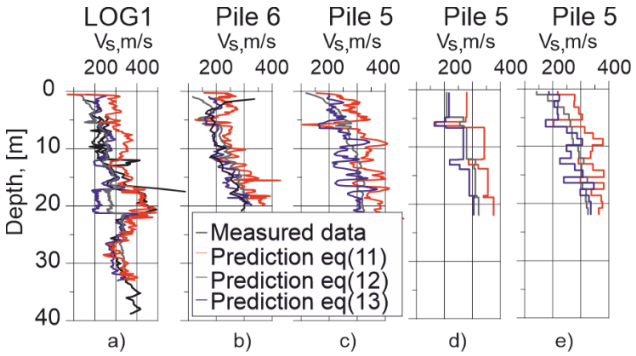

Figure 3. (a, b). Comparison of in-situ measured and predicted V_s using published (11, 12) and locally derived (13) correlation. c) V_s- Prediction for the location P5; (d) averaging of the velocity predicted at P5 over geological layers from Figure 1; (e) averaging over 1 m intervals.

Driving rate as a function of the shear wave velocity was calculated at the frequencies f = 18, 20, 22 and 24 Hz. The strengths of both the pile shaft and pile tip were kept constant and independent of the shear wave velocity.

The velocity profile calculated according to the equation (13) and averaged over stratigraphic layers is further referred to as the base case (Fig. 3d). The driving rate calculated for this profile was compared to the driving rates in three cases listed below: Case 1) Stiffness factor: reduced and increased stiffness. Stiffness factors were arbitrary chosen ranging from 0.5 to 1.5. The "stiffer" and "softer" profiles were calculated by multiplying the base case velocity by a constant stiffness factor. Case 2) Profiles obtained using different empirical relationships and averaging approaches. Velocities obtained using equations (11), (12) and (13) were averaged over either stratigraphic units or 1 m depth intervals; Case 3) Profiles obtained for different embedded length.

Figure 4 displays the sensitivity of the driving rate to the soil stiffness. The trice increase of the shear wave velocity provokes the decrease of the driving rate by approximately 40% to 50% by different frequencies. The highest driving rate is achieved for the frequencies 20-24 Hz, which coincides very well with the in-situ data. At lower stiffness the driving rate tends to stay constant, and the lowest frequencies provide highest penetration. Figure 5 presents the influence of different empirical relationships. Use of equation (12) leads to the lowest driving rate most likely due to overestimation in the velocities. The differences in results due to application of equations (11) and (12) are of the order of 10 % and are considered minor in view of other uncertainties. This fact allows to conclude that the correct choice of a published empirical relationship would be sufficient for initial stage of drivability prognosis.

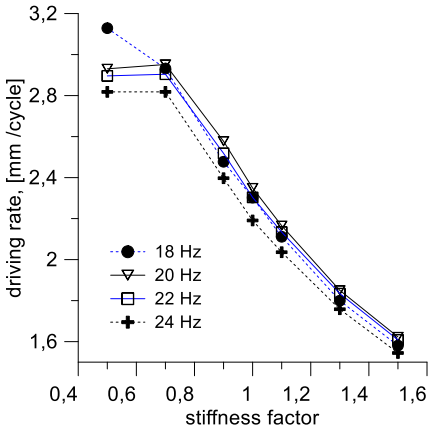

Figure 4. Driving rate as a function of stiffness.

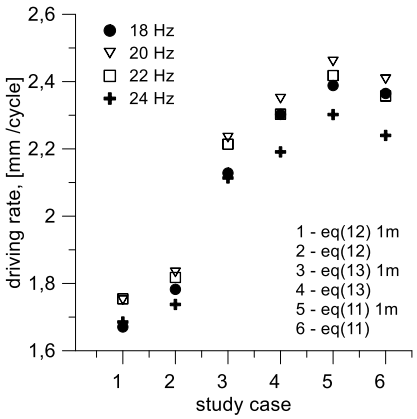

Figure 5. Influence of the chosen empirical relationship on the driving rate

The figure 6 displays the decrease of the driving rate with increasing embedded length. This behavior could be explained due to changed overall shaft resistance. However, the change of the optimum frequency with stiffness needs to be further investigated.

6 RESULTS AND DISCUSSION

As expected, a decrease of the shear wave velocity leads to an increase of the driving rate as shown on Figure 4 due to decrease of the dynamic stiffness of the pile. At the same time, as the damping also decreases, the differences in driving rate with frequency become more pronounced for softer profiles. The frequency needed to achieve highest penetration changes with shear wave velocity which reflects the effect of both, the shear modulus G, and the damping D. This is in agreement of theoretical basis but has to be further investigated in detail.

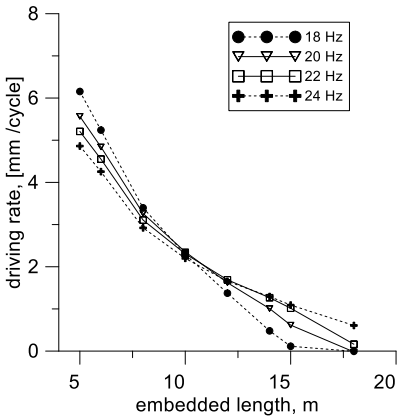

Figure 6. Driving rate as a function of embedded length

A local empirical relationship to derive V_s from CPT data was proposed here. Application of the different empirical relationships to calculate V_s reveals the same tendencies for driving rate. Different averaging approaches influence the results only insignificantly.

The shown influence of the embedded length L on the driving rate (Figure 6) can be explained with the corresponding change of the overall shaft resistance. However, the change in the optimum frequency with L needs to be studied in more detail.

The numerical code can readily be modified to simulate continuous pile penetration by vibration by simply including new penetrated layers; however, this has not been attempted for practical purposes yet. The key point is that we have shown that taking known initial soil conditions into account, the numerical code predicts the choice of the optimal vibration frequency as a function of soil stiffness.

At the same time a useful practical observation was made that the choice of an empirical relationship to estimate the V_s will not affect the results significantly.

During the in-situ installation the last 10 m of the pile were installed at the frequency of 22.5 Hz within 90 s. This corresponds to the driving rate of 9.3m/22.5Hz/90s = 4.6 mm/s. This is approximately twice as high as the predicted driving rate for the same velocity profile. Considering that the yield strength of the pile-soil springs is the most uncertain parameter and no special investigation were made in the current research the prediction is in overall good agreement with the in-situ values. A liquefaction due to vibratory installation may decrease the pile-soil friction angle dramatically which leads to a rapid increase in driving rate. See Kaynia (2022) for details.

7 CONCLUSIONS AND OUTLOOK

This article describes the process of parameter estimation for the numerical code *VibPile* to predict vibratory pile installation. The code applies a minimum number of input soil parameters such as interface friction angle, shear wave velocity and soil density. All parameters have a clear geomechanical sense and can be estimated using established laboratory tests or empirical relationships.

For wind farm development, the shear wave velocity is unlikely to be measured at every pile location, therefore, it must be determined from CPT data using published or local empirical relations. Even more likely is the case when the windfarm layout has been changed after the geotechnical campaign and most of the CPT measurements must be interpolated to unexplored locations. In this case, the accuracy of the V_s estimations decreases even more. As shown here, the numerical code *VibPile* is applicable for the choice of penetration frequency even if the uncertainty in the shear wave velocity is on the order of 50%. This decreases the installation time and saves offshore operation costs.

Further automation accounting for the increase in the embedded length, the differences of the interface friction angle with relative density as well as its change during penetration will increase the accuracy of the predictions and allow reaching a better agreement between in-situ and numerical results.

ACKNOWLEDGEMENTS

The work was partially financed by the grant Nr 0324231B by the German ministry of economic affairs. Authors thank Yunsup Shin for his comments at the early stage of this work.

REFERENCES

1. Biryaltseva, T., Lunne, T., Kreiter, S. & Moerz, T. (2016). Relative density prediction based on in-situ laboratory measurements of shear wave velocity. In Lehane, B. et al. (eds), *Geotechnical and Geophysical Site Characterisation 5, Proc. Int. Conf. ISC'5, Gold Coast, 5-9 September 2016*, 1: 389-394.

2. Busch A.V., Kluger, M.O, Mörz, T. (2022) Corrosion effects on axial pile capacity. *Engineering Geology (Submitted).*

3. Crispin, J.J. and Mylonakis, G.E. (2021). Simplified models for axial static and dynamic analysis of pile foundations in Analysis of Pile Foundations Subject to Static and Dynamic Loading, Kaynia, A.M. (Ed.), CRC Press, London.

4. Gattermann, J., Herwig, V. & Moormann, C. 2015. VIBRO Projekt Vergleich des lateralen Tragverhaltens von vibrierten und geschlagenen Stahlrohrpfählen in sandigen Böden. Pfahl-Symposium 2015, Mitteilungen des Instituts für Grundbau und Bodenmechanik, Technische Universität Braunschweig, Heft 99 (in German).

5. Kaynia A.M., Hebig J., Pein, T., Shin, Y. (2022) Numerical model for dynamic installation of large diameter monopiles. *Soil Dynamics and Earthquake Engineering, 161 (in press)*

6. Mayne, P.W. (2007) NCHRP synthesis 368. Cone Penetration Testing. A synthesis of highway practice, Washington, D.C.: transportation research board.

7. Novak, M. (1974). Dynamic stiffness and damping of piles. Canadian Geotech. J., 11(4):574-598.